ORIGINAL ARTICLE

The effects of pH, surfactant, ion concentration, coformer, and molecular arrangement on the solubility behavior of myricetin cocrystals ☆

Shuzhen Ren[a,†], Mingyu Liu[a,b,†], Chao Hong[a], Guowen Li[c], Jiabin Sun[a], Jianying Wang[d], Lei Zhang[d], Yan Xie[a,*]

[a]Research Center for Health and Nutrition, Shanghai University of Traditional Chinese Medicine, Shanghai 201203, China
[b]Institute of Chinese Materia Medica, Shanghai University of Traditional Chinese Medicine, Shanghai 201203, China
[c]Pharmacy Department, Shanghai TCM-Integrated Hospital, Shanghai University of Traditional Chinese Medicine, Shanghai 200082, China
[d]Shanghai Innovation Center of TCM Health Service, Shanghai University of Traditional Chinese Medicine, Shanghai 201203, China

Abstract Pharmaceutical cocrystals are a promising technology that can be used to improve the solubility of poor aqueous compounds. The objective of this study was to systematically investigate the solubility of myricetin (MYR) cocrystals, including their kinetic solubility, thermodynamic solubility, and intrinsic dissolution rate (IDR). The effects of pH, surfactant, ion concentration, and coformers on the cocrystal solubility were evaluated. Furthermore, single crystal structures of MYR, myricetin–isonicotinamide (MYR–INM) and myricetin–caffeine (MYR–CAF) cocrystals were analyzed to discuss the possible reasons for the enhancement of cocrystal solubility from the perspective of the spatial structure. The results indicated that the kinetic solubility of MYR cocrystals was modulated by pH and cocrystal coformer (CCF) ionization in buffer solution, while it primarily depended on the CCF solubility in pure water. In addition, the solubility of MYR cocrystals was increased in a concentration dependent fashion by the surfactant or ion concentration. The thermodynamic solubility of MYR–INM (1:3) cocrystals decreased with the increases of the pH value of the dissolution media. The IDR of MYR cocrystals was faster than that of MYR in the same medium and extremely fast in pH 4.5 buffer. The improved solubility

of MYR cocrystals was probably related to the alternate arrangements of MYR and INM/CAF molecules and increased intermolecular distance. The present study provides some references to investigate the solubility behavior of pharmaceutical cocrystals.

1. Introduction

Pharmaceutical cocrystals are defined as a multi-component system that contains an active pharmaceutical ingredient (API) and cocrystal coformer (CCF) at a specific stoichiometric ratio that are linked *via* intermolecular interactions, such as hydrogen bonds, π–π packing, and van der Waals forces[1–3]. As a promising formulation, pharmaceutical cocrystals can improve some of the physicochemical properties of APIs, such as the solubility, dissolution rate, bioavailability, and stability, without altering their inherent chemical structures[4,5]. For instance, the solubility of quercetin in quercetin–caffeine cocrystals was enhanced nearly 14 times in a 1:1 ethanol/water medium compared with that in pure quercetin, and its oral bioavailability was enhanced 2.6 times by quercetin–caffeine cocrystals[6]. Under the conditions of the accelerated stability test, temozolomide is converted to temozolomide hydrate (from light pink to brown) within 1 month, while cocrystals of temozolomide with succinic acid retain their initial crystal form and color for up to 6 months, indicating that the stability of temozolomide is strengthened by its cocrystal form[7]. Meanwhile, the guidance for industry regulatory classification of pharmaceutical cocrystals announced by the U.S. Food and Drug Administration (FDA) claims that cocrystals, as a drug product intermediate or a fixed-dose combination product, should substantially dissociate before reaching the site of pharmacological activity[8,9]. Actually, cocrystals are meta-stable solids because of their weak intermolecular interaction and easily dissociate into their respective components in solution[10,11]. However, thus far, it remains unclear whether and when cocrystals will transform into their corresponding starting materials prior to taking effect and how the related factors influence the transformation behavior. Therefore, it is essential to explore the detailed behaviors of pharmaceutical cocrystals between their dissolved and dissociated processes, which will be beneficial to advance the development and application of pharmaceutical cocrystals.

Pharmaceutical cocrystal solubility commonly comprises a dissolution–dissociation process, and its evaluation is based on kinetic solubility, thermodynamic solubility, and the intrinsic dissolution rate. Kinetic solubility usually indicates a dynamic process such that the concentration fluctuations vary with time during cocrystal dissolution and depends on parameters such as the surface area, particle size and distribution, fluid dynamics, and experimental apparatus[12]. However, thermodynamic solubility focuses on the dissolved extent of the cocrystal when all the cocrystal components achieve dynamic equilibrium in the solution phase entirely[13]. The intrinsic dissolution rate concentrates on how the powder compacts affect the drug dissolution under a constant temperature and surface condition, which will contribute to approximately simulating the *in vivo* behavior of drug formulation[14]. Consequently, the above mentioned provide the feasible measures to reveal the phase behavior of cocrystals in solution from various aspects. As is well known, solvation is a vital factor for the cocrystal dissolution–dissociation process in the human gastrointestine that is related to coformer solubility, the type and concentration of

surfactants, and the ion concentration in dissolution media[15]. In addition, cocrystal solubility is influenced by the strength of the crystal lattice that is associated with the crystal-stacked form and intermolecular distance of API and CCF[16]. Thus, it is worthy to understand the diverse mechanisms of cocrystal solubility to further gain insight into the inherent nature of cocrystals and propose the design of cocrystals rationally.

Myricetin (MYR), 3,3′,4′,5′,5,7-hexahydroxyflavone, which widely exists in various plants, such as blackcurrants, red wine, cranberries, and broad beans, is a flavonoid compound with 6 phenolic hydroxyl groups; MYR has many pharmacological activities, including antiin-flammatory, antiallergic, antiplatelet aggregation, and antioxidant effects[17,18]. Our previous research showed that MYR was poorly absorbed in the human body orally (the absolute bioavailability of MYR in rats is only 9.62%), likely due to its low aqueous solubility in water (16.6 μg/mL)[19,20]. Fortunately, the exterior functional groups in the chemical structure of MYR are amenable to form supramolecular heterosynthons and engage in hydrogen bonding sequentially; thus, the cocrystal technique has been undertaken to address the solubility issue of MYR[21]. Currently, a series of MYR cocrystals with proper coformers, such as caffeine, piracetam, nicotinamide, isonicotinamide, acetamide, 4,4′-bipyridine, proline, and 4-cyanopyridine, has been synthesized, and some of MYR cocrystals can significantly increase the solubility of MYR[22–27]. For instance, the apparent solubility of myricetin–acetamide cocrystals is 40 μg/mL in ∼27 min and increases thereafter persistently, whereas that in pure MYR is only 10 μg/mL invariably; a similar behavior investigation of myricetin–proline cocrystals showed that the maximum solubility value is 7.25 μg/mL in 40 min, which is increased by 7.69 times that of raw MYR. Nevertheless, none of these reports provided systematic investigation on the solubility behavior of MYR cocrystals, hindering the realization of the great usefulness of MYR cocrystals.

Therefore, in the present study, the solubility behavior of MYR cocrystals, such as the kinetic solubility, thermodynamic solubility, and intrinsic dissolution rate, was explored. Briefly, the influence of CCFs, pH values, surfactants, and the ion concentration on cocrystal solubility was determined, and the solution stability of MYR cocrystals was investigated by simultaneously monitoring the solid-state changes with powder X-ray diffraction (PXRD). Moreover, the bond length and molecular arrangements of the obtained crystal structures of the cocrystals were analyzed by single-crystal X-ray diffraction to preliminarily elucidate the effects of spatial structure on cocrystal solubility.

2. Materials and method

2.1. Materials

The raw MYR was purchased from Shanghai DND Pharm-Technology Co., Inc. (Shanghai, China). Nicotinamide (NIC),
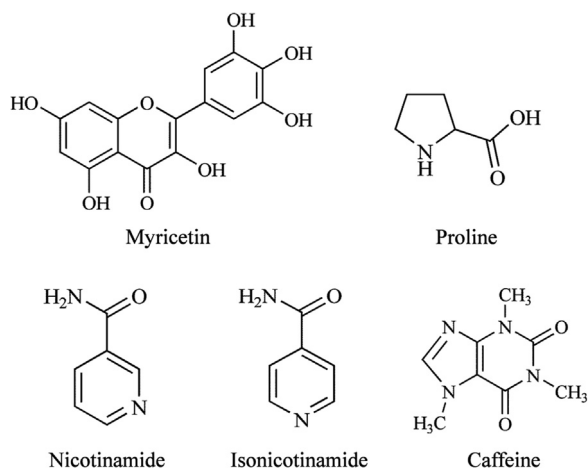
Figure 1 Chemical structures of myricetin (MYR) and coformers.

isonicotinamide (INM), caffeine (CAF), proline (PRO), and lecithin were obtained from Aladdin Co., LLC. (Shanghai, China). Ethanol, Tween-80, and sodium dodecyl sulfate were purchased from Sinopharm Chemical Reagent Co., Ltd. (Shanghai, China). Kolliphor p188 and Cremophor ELP were donated by Shanghai Yunhong Chemical Preparation Auxiliary Technology Co., Ltd. (Shanghai, China). Chemicals were used as received from the companies without further purification. All analytical grade solvents were purchased from Binghua Biochemical Co., Ltd. (Shanghai, China).

2.2. Cocrystal preparation

The chemical structures of MYR and coformers are presented in Fig. 1 and the MYR–NIC, MYR–INM, MYR–CAF, MYR–PRO cocrystals were prepared as described in our previous publications[22,27].

Single crystals were obtained by the solvent evaporation method using common laboratory solvents. MYR single crystals were prepared by adding excess MYR to methanol (6 mL), followed by sonication until complete dissolution. After filtration, a small amount of water was added dropwise and evaporated at room temperature. Two days later, a yellow crystal was obtained. MYR–CAF single crystals were prepared by adding excess MYR powder to nearly saturated solutions of CAF in methanol (8 mL), followed by shaking for 24 h at room temperature. The filtrate was evaporated at ambient temperature. After 16 days, a tawny crystal was harvested. The MYR–INM single crystal was prepared by adding ~400 mg of INM to 10 mL of methanol to obtain a saturated solution and was filtered to remove excess INM. Next, an excess amount of MYR was added to the above saturated solution. The resulting suspension was shaken for 12 h in a water bath at room temperature and was then subjected to filtration. After two days, a light-yellow crystal was also acquired by slowly evaporating the final filtrate. All the crystals were suitable for single-crystal X-ray diffraction analysis.

2.3. Kinetic solubility measurement

Solubility studies for MYR, MYR–NIC, MYR–INM, MYR–CAF, and MYR–PRO cocrystals in the various media were investigated using the classical saturation shake-flask method. Briefly, the solids were dried under vacuum and sieved through 80-mesh sieves. Powder

equivalents of 30 mg of MYR were added to 10 mL of dissolution medium of distilled water, hydrochloric acid solution (pH 1.2), acetate buffer solution (pH 4.5), and phosphate buffer solution (pH 6.8), respectively. Next, the resultants were placed in a CHA-S air-bath thermostatic shaker-incubator (Meixiang Instruments Co., Ltd., Shanghai, China) at $37 \pm 0.5\,°C$. The solutions were agitated constantly at a rate of 200 rpm, and 1 mL of sample was withdrawn at predetermined time intervals (12, 24, 36, and 48 h) and was then filtered through a 0.45-μm hydrophilic membrane filter and centrifuged at 13,000 rpm (Heraeus Multifuge X1R centrifuge, ThermoFisher Scientific, Waltham, USA) for 10 min. Subsequently, a 20 μL of supernatant was injected into an HPLC system to quantify the concentration of MYR[20]. Additionally, the influence of surfactants (0.5% Tween-80, 0.5% Cremopher EL) and the ion concentrations (219.5, 400, and 600 mmol/L acetate buffer solutions) on cocrystal solubility were determined by the same method. All experiments were performed in triplicate. Ultimately, the remaining solid materials after the above-mentioned solubility studies were stored, dried at $40\,°C$, and examined for phase transformation by powder X-ray diffraction (PXRD).

2.4. Transition concentration (C_{tr}) measurement

Measurements of the cocrystal C_{tr} values were performed by adding excess cocrystal to the saturated drug solution. Briefly, ~50 mg of MYR was dissolved in 5 mL of distilled water, a hydrochloric acid solution (pH 1.2), acetate buffer solution (pH 4.5), and phosphate buffer solution (pH 6.8); and then, the mixture was shaken at 200 rpm for 24 h in an HZS-H thermostated water bath (HDL Apparatus, Harbin Donglian Electronic Technology Development Co., Ltd., Beijing, China) at $37\,°C$. Thereafter, the MYR cocrystals (~100 mg) were added to the above MYR suspension and stored under continuous shaking for 24 h. All experiments were performed in triplicate. Eventually, the supernatants were filtered through 0.45-μm membrane filters and the concentration of MYR and CCFs were separately quantified by the HPLC assay[20]. Particularly, the remaining solid phases were collected and dried at $40\,°C$ and were characterized to confirm the composition of the residual solid by PXRD.

2.5. Intrinsic dissolution rate determination

The intrinsic dissolution rate (IDR) test of all solid-state forms of MYR were performed using the dissolution device FODT-101G (Fu Kesi analysis instrument Co., Ltd., Shanghai, China). One hundred milligrams of each solid powder (MYR, MYR cocrystals) were weighed and compressed in an 8-mm punch three times. The tablet die was set at a pressure of 150 kg for 2 min. The intrinsic dissolution device containing the tablet is mounted on an optical fiber dissolution apparatus and was separately immersed into 700 mL of 0.5% Tween-80, hydrochloric acid solution (pH 1.2), acetate buffer solution (pH 4.5), or phosphate buffer solution (pH 6.8) at $37\,°C$ with the paddle rotating at 300 rpm. All experiments were performed in triplicate. The absorbance of light (380 nm) was continuously monitored using a UV–Vis fiber optic probe connected to a computer and was terminated after 60 min. The absorbance data were converted into MYR concentrations using a previously constructed calibration curve to obtain the MYR concentration-time profiles. IDR was obtained as the ratio of the slope of the initial linear portion on the dissolution curve and tablet surface area exposed to the dissolution medium.

2.6. Powder X-ray diffraction (PXRD)

Powder X-ray diffraction was recorded on the Ultima IV X-ray diffractometer equipped with a D-TEX detector and a monochromatic Cu K$_\alpha$ radiation ($\lambda = 1.54$ Å, Rigaku Corporation, Tokyo, Japan) at a voltage of 40 kV and a current of 40 mA. Each sample was scanned over a 2 theta range of 3–50° with a step size of 0.01 °/s and a scan speed of 6 °C/min.

2.7. Single-crystal X-ray diffraction and refinements

Single-crystal X-ray diffraction data collection of the MYR and MYR cocrystals was performed using a Bruker Apex II CCD diffractometer (Bruker Scientific Technology Co., Ltd., Karlsruhe, Germany) with graphite-monochromated Mo K$_\alpha$ radiation ($\lambda = 0.71073$ Å) at 293 K. The crystal structures were solved by direct methods and were refined by the full-matrix least-squares method using the SHELXL-97 crystallographic software package. All the non-hydrogen atoms were refined anisotropically, and the hydrogen atom positions were calculated geometrically, refined using a riding model. Diamond 3 was used for molecular representations and packing diagrams. Crystallographic data in the cif format have been deposited in the Cambridge Crystallographic Data Center, CCDC No. 1409763, 1493056, 1409762 for MYR, MYR-CAF, and MYR-INM cocrystals, respectively.

3. Results and discussion

3.1. Kinetic solubility and solution stability

3.1.1. Effects of pH on the kinetic solubility and solution stability

The dynamic solubility profiles for MYR–PRO, MYR–NIC, MYR–INM, and MYR–CAF cocrystals in water and buffer solutions are shown in Fig. 2, and PXRD patterns of the residual solid obtained from the apparent solubility of MYR cocrystals are presented in Figs. 3 and 4.

For the MYR–PRO cocrystals, the solubilities in water, pH 1.2, and pH 4.5 at 12 h achieved maximum values (63.93, 13.16, and 14.12 µg/mL, respectively) and subsequently reached a plateau, while the solubility was only 2.90 µg/mL at 12 h in pH 6.8 buffer, followed by a slow but steady increase (Fig. 2A). Obviously, the maximum solubility value of MYR–PRO cocrystals in water is at least 4-fold greater than that in other buffer solutions, which might be explained by the diffusion principle and inherent nature of PRO. Specifically, the concentration of the dissolving PRO at the diffusion interface is higher than that of MYR after the cocrystal was dissociated because of the following two reasons: (1) the PRO molecule diffuses in water faster than MYR because the molecular weight of PRO is smaller than that of MYR; (2) PRO possesses a strong affinity to water molecules owing to its zwitterion nature[28]. Consequently, the less soluble MYR molecules become supersaturated in water and aggregate as an amorphous phase[29], resulting in the maximum peak solubility attained in water. Additionally, the minimum solubility of the MYR–PRO cocrystal was observed in pH 6.8 buffer, which is likely ascribed to the hydroxyl ion from pH 6.8 buffer can induce the ionization of PRO, thus inhibiting MYR–PRO cocrystal dissociation and delayed phase transformation[30]. Moreover, MYR is unstable when the concentration of hydroxide ions is relatively high in media[20], which is also a reason for the low solubility of MYR–PRO

cocrystal in pH 6.8 buffer. The similar impact of CCF ionization on cocrystal solubility was discussed in other works[31,32], which can also support the viewpoint obtained in the present study.

As shown in Fig. 3A, most crystalline peaks are consistent with MYR in the residual solid after MYR–PRO cocrystals are solubilized in the four media for 48 h, indicating that MYR–PRO cocrystals undergo phase transitions and are unstable in these media. To adequately elucidate phase transformation behavior during the dissolution–dissociation process, the composition of residual solid at different time points were examined by PXRD. For water and pH 1.2 buffer (Fig. 4A and B), most crystalline peaks of the residual solid were consistent with that of MYR, and the diffraction intensities were increased over time (from 4 to 48 h), suggesting that MYR–PRO cocrystal has converted into MYR at 4 h. Interestingly, the intensity of the characteristic peaks at 6 h in pH 1.2 buffer is much stronger than that in water, indicating that the cocrystal dissociation rate is faster in pH 1.2 buffer than that in pure water, probably due to the hydrogen ions in the acidic medium accelerating MYR–PRO cocrystal dissociation and providing the driving force for the nucleation and growth of MYR[33]. In pH 4.5 buffer (Fig. 4C), however, only one broad diffraction peak was observed at 4 h, and the characteristic peaks of MYR appeared at 6 h, implying that the cocrystal undergoes transformation from the metastable phase to the unstable amorphous phase and then to the stable phase during the dissolution process[10,34]. Regarding the pH 6.8 buffer (Fig. 4D), no obvious characteristic peak was observed within 12 h, but characteristic peaks of MYR appeared at 24 h, indicating that MYR–PRO cocrystals remained in the amorphous state for a long time, and, consequently, the cocrystal solubility kept increasing as presented in Fig. 2A. The delayed phase transformation was presumably attributed to the hydroxyl ion hindering the breakage of the intermolecular hydrogen bond in pH 6.8 buffer.

For the other three cocrystals, the maximum apparent solubility values of the MYR–NIC cocrystal reached at 12 h in water, pH 1.2 buffer, and 4.5 buffer (28.30, 29.08, and 43.84 µg/mL, respectively) and followed by an obvious decline after 12 h (Fig. 2B); similar dissolution behavior was also observed in MYR–INM and MYR–CAF cocrystals (Fig. 2C and D). Additionally, the solubility of the three MYR cocrystals in pH 4.5 buffer was coincidently higher than that in other aqueous solutions, probably related to the solubility of MYR cocrystals being dominated by the solubility of MYR, which is pH dependent and has high solubility in pH 4.5 acetate buffer[27]. Additionally, the "spring and parachute" phenomenon was obviously observed in those profiles, probably resulting from the cocrystals dissociating into less soluble MYR in solution[10]: the hydrophobic MYR molecules become supersaturated and exist as the high-energy form in aqueous solutions, known as "spring", and inhibiting the rapid precipitation of MYR is related to "parachute".

The PXRD characteristic peaks of MYR appeared in the residual solid obtained from water and the pH 1.2 solution (Fig. 3B, g and f), but the strength of the characteristic peaks in water was weak compared with that in pH 1.2 solution, indicating that the MYR–NIC cocrystal was partially decomposed into individual component in water but completely decomposed in pH 1.2 buffer. The cause may be that the nucleation and/or growth rate of the MYR crystalline phase was faster in pH 1.2 buffer than in water. A similar phase transformation was observed in MYR–INM cocrystals (Fig. 3C, f), while characteristic peaks of MYR and MYR–INM cocrystals were all observed (Fig. 3C, g). For the pH 4.5 buffer, no distinct characteristic peaks appeared (Fig. 3B, e), indicating the residual solid is amorphous, and, thus, the MYR–NIC cocrystal was unstable
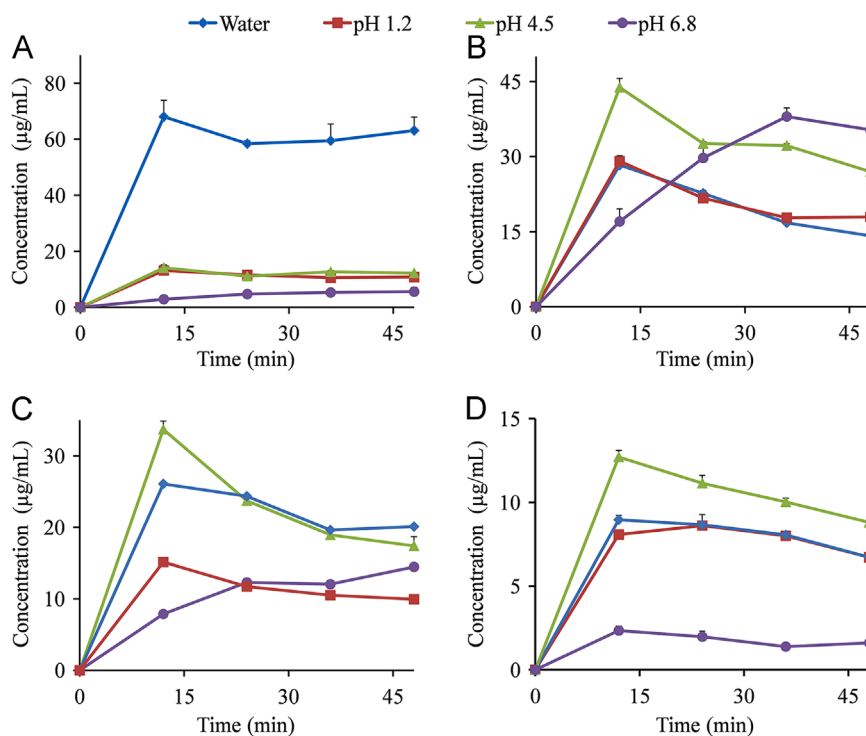
Figure 2 Dynamic solubility profiles for MYR–PRO (A), MYR–NIC (B), MYR–INM (C), and MYR–CAF (D) cocrystals in water (♦) and aqueous solution at pH 1.2 (■), pH 4.5 (▲), pH 6.8 (●) ($n = 3$).
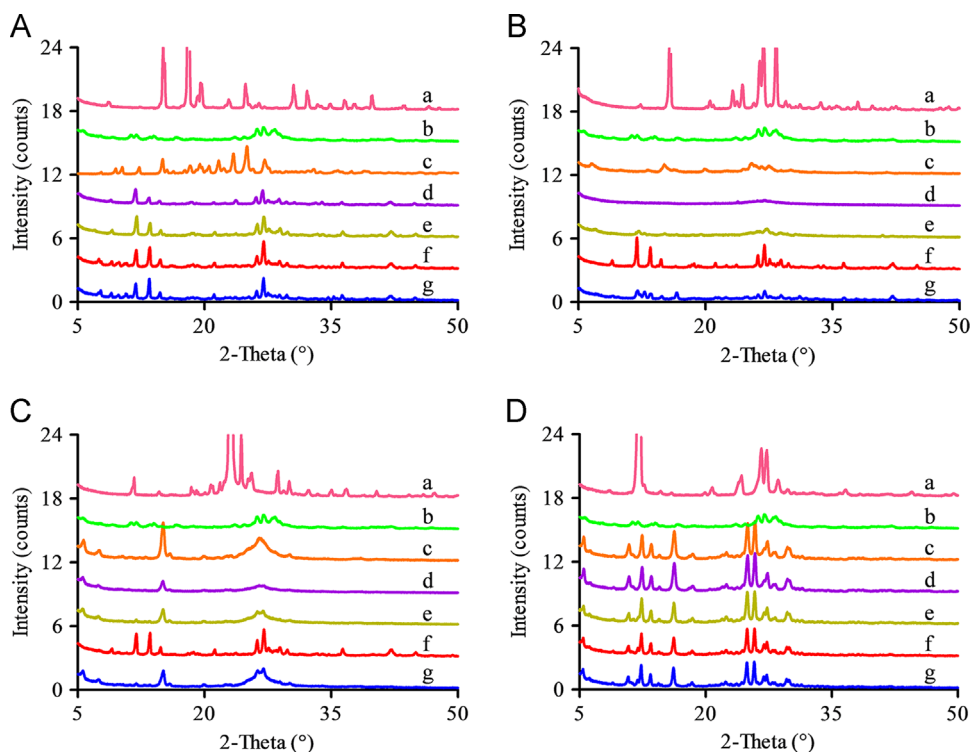
Figure 3 PXRD patterns of the residual solid obtained from the apparent solubility of MYR–PRO cocrystal (A), MYR–NIC cocrystal (B), MYR–INM cocrystal (C), and MYR–CAF cocrystal (D) at 48 h, which were performed in buffer solutions at pH 6.8 (d), pH 4.5 (e), pH 1.2 (f), and water (g), respectively. The PXRD patterns of the corresponding CCF (a), MYR (b), and the initial MYR cocrystal (c) were also given to confirm the composition of the residual solid.
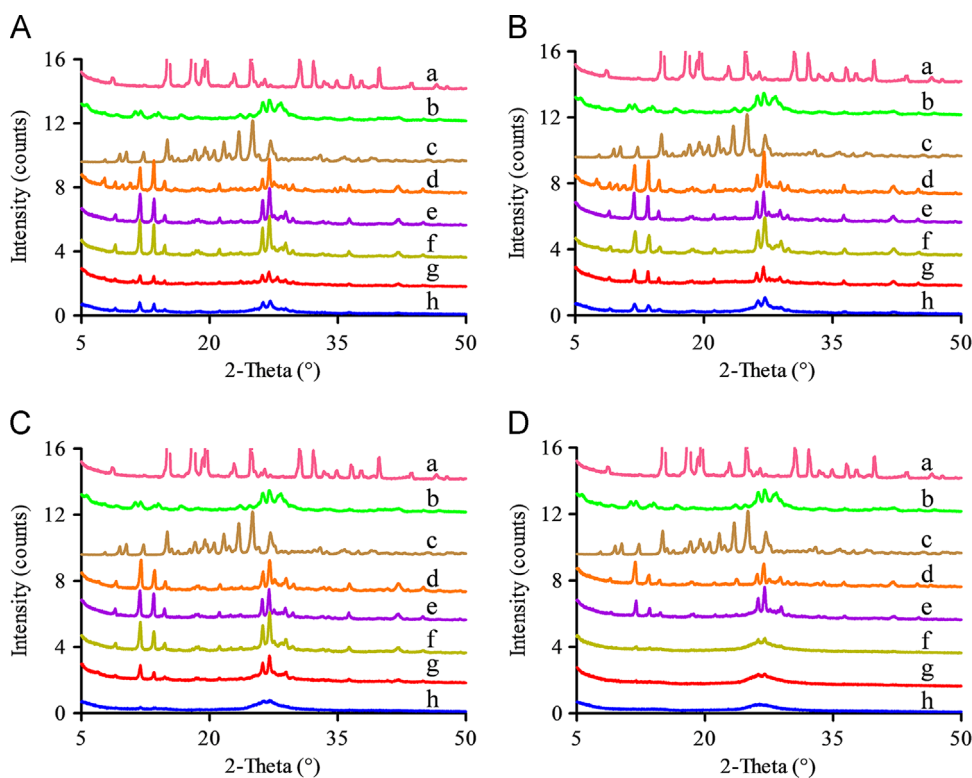
Figure 4 PXRD patterns of the residual solid obtained from the apparent solubility of MYR–PRO cocrystal, which was performed in water (A) and buffer solutions of pH 1.2 (B), pH 4.5 (C), and pH 6.8 (D) at 4 h (h), 6 h (g), 12 h (f), 24 h (e), 48 h (d), respectively. The PXRD patterns of the corresponding PRO (a), MYR (b), and MYR-PRO cocrystal (c) were also given to confirm the composition of the residual solid.

in this medium. By contrast, the characteristic peaks of the MYR–INM cocrystal were observed (Fig. 3C, e), indicating the MYR–INM cocrystal was more stable than the MYR–NIC cocrystal.

However, continuously increased solubility in pH 6.8 buffer was observed for MYR–NIC and MYR–INM cocrystals (Fig. 2B and C), probably due to the high hydroxyl ion concentration in pH 6.8 medium induced by NIC and INM (their pK_a values are 10.4 ± 0.5 and 10.61 ± 0.5, respectively, from SciFinder predicted data) that decreased the dissociation rate of these two cocrystals. In addition, no characteristic peaks were observed at 48 h (Fig. 3B, d), indicating that the MYR–NIC cocrystal showed phase transformation but did not convert to stable MYR crystals. However, several characteristic peaks of MYR–INM cocrystal appeared (Fig. 3C, d), reflecting that incomplete phase transformation occurred. The above solubility and PXRD pattern results also suggested that the dissociation rate of MYR–NIC and MYR–INM cocrystals in pH 6.8 buffer solution was slow and the dissolve–dissociate process would be maintained for a long time.

For the MYR–CAF cocrystal, a low aqueous solubility was demonstrated in the testing media and extremely low in pH 6.8 buffer solution (Fig. 2D), and the corresponding remaining crystalline peaks were consistent with MYR–CAF cocrystals (Fig. 3D), indicating that the cocrystal possess equal or lower solubility than MYR or CAF. Such a phenomenon also demonstrated that the solid phase transformation extent was below the detection limit of PXRD, and the MYR–CAF cocrystal was stable in the investigated media.

In summary, the solubility and stability of MYR cocrystals are influenced by the pH value of the buffer solution, and their dissolution–dissociation process is closely related to the phase transformation. The high concentration of hydrogen ions (low pH)

provided the driving force for phase transformation and facilitated MYR cocrystal dissociation, indicating that the cocrystal is thermodynamically unstable at low pH. Conversely, the high concentration of hydroxyl ions (high pH) impeded the breaking of intermolecular hydrogen bonds and MYR cocrystal dissociation, which were related to CCF ionization and the degradation of API at high pH.

3.1.2. Effects of CCFs on the apparent solubility

The impact of CCFs on the apparent solubility of MYR cocrystals were analyzed as shown in Fig. 1. In water, as the ionization effect can be ignored[35], the solubility of MYR cocrystals is mainly dependent on the corresponding CCF solubility—i.e., the solubilities of MYR–PRO, MYR–NIC, MYR–INM, MYR–CAF cocrystals at 12 h are 63.93 ± 10.71, 28.30 ± 0.38, 26.07 ± 0.25, and 8.08 ± 0.22 μg/mL, respectively (Fig. 2)—which is consistent with the aqueous solubility order of CCFs in water at 25 °C: PRO (2.22 mol/L) > NIC (0.36 mol/L) > INM (0.35 mol/L) > CAF (0.30 mol/L) (Scifinder data). Additionally, the order of the stability of MYR cocrystals was displayed as follows: MYR–CAF > MYR–INM ≈ MYR–NIC > MYR–PRO (Fig. 3). Thus, it can be inferred that the stability of MYR cocrystals was negatively correlated with the CCF solubility. Similar to our findings, the stability of Gabapentin–3HBA cocrystals was also inversely related to its solubility[36]. However, in the case of buffer solutions, the cocrystal solubility was generally influenced by the ionization of CCFs because the pH at the dissolving surface can be modulated by the pK_a values of CCFs and, thus, is different to the bulk pH[15,37]. Nevertheless, in pH 1.2 and 4.5 buffers, the ionization effect on the cocrystal solubility was inconspicuous. Consequently, the high hydrogen ion concentration (pH 1.2) and
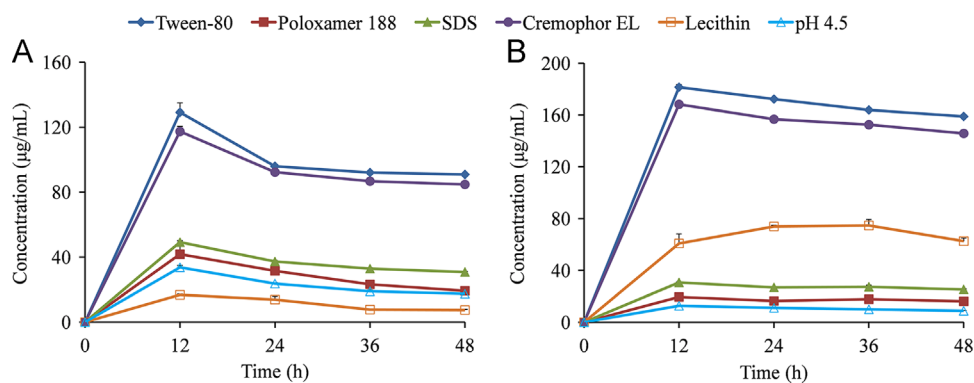
Figure 5 Apparent solubility of MYR–INM (A) and MYR–CAF (B) cocrystals in the pH 4.5 buffer containing different surfactants of Tween-80 (◆), Poloxamer 188 (■), SDS (▲), Cremophor EL (●), Lecithin (□), and the blank buffer solution (△) ($n = 3$).
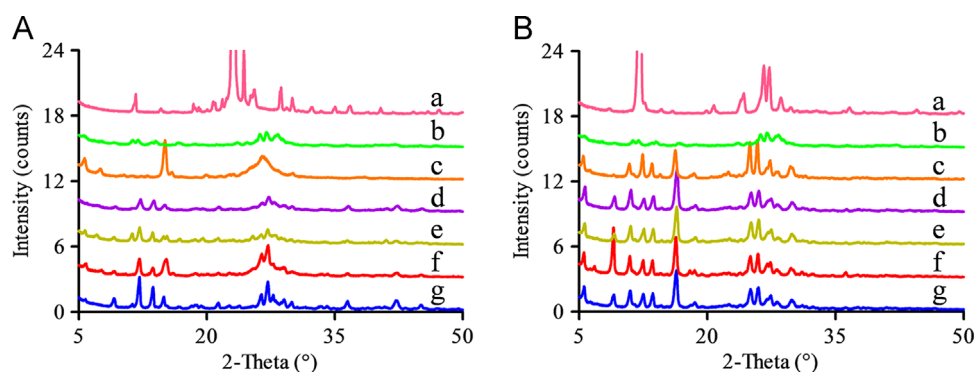
Figure 6 PXRD patterns of the residual solid obtained from the apparent solubility of MYR–INM cocrystal (A), MYR–CAF cocrystal (B), which were performed in the pH 4.5 buffer containing 0.5% of Tween-80 (d), Cremophor EL (e), SDS (f), and Poloxamer 188 (g), respectively. The PXRD patterns of the corresponding CCF (a), MYR (b), and the initial MYR cocrystal (c) were also given to confirm the composition of the residual solid.

pH-dependent solubility of MYR (pH 4.5) governed the MYR cocrystal solubility as described in Section 3.1.1. In pH 6.8 medium, the ionization of CCFs induced by their pK_a values was the dominating factor for the dissolution behavior of MYR cocrystals.

3.1.3. Effects of surfactants on the apparent solubility

Although MYR–INM and MYR–CAF cocrystals displayed the maximum apparent solubility at 12 h in pH 4.5 buffer, they did not completely convert to individual components. Because adding surfactants to aqueous media increases the solubility of both cocrystals and their constituent APIs, thereby facilitating cocrystal dissociation[38], some surfactants, such as lecithin and taurocholate, exist in gastrointestinal fluids[39]; the effects of surfactants on the apparent solubility of MYR–INM and MYR–CAF cocrystals were investigated in the following experiments.

As shown in Fig. 5A, the maximum solubility values of MYR–INM cocrystals in pH 4.5 buffer containing 0.5% Tween-80, Cremophor EL, SDS, and Poloxamer 188 were 3.8-fold, 3.5-fold, 1.46-fold, and 1.24-fold higher than those in pH 4.5 buffer. However, the solubility of MYR–INM cocrystals in pH 4.5 buffer containing 0.5% lecithin was lower than that in pH 4.5 buffer. This phenomenon indicated that all the above surfactants, except for lecithin, enhanced the solubility of MYR cocrystals, probably due to lecithin at the present concentration exhibiting a relatively weak interplay with MYR or INM so that MYR–INM cocrystals could

not be dissociated and, thus, showed low cocrystal solubility[40]. In addition, both characteristic peaks of MYR and MYR–INM cocrystals appeared in the residual solid (Fig. 6A), demonstrating that the incomplete phase conversion of cocrystal occurred even if the surfactants were present in the dissolution media. Interestingly, the intensity of the crystalline peaks of the residual solid obtained after the apparent solubility experiment of MYR–INM cocrystals in SDS buffer were similar to those in Poloxamer 188 buffer but different from those in Tween-80 buffer or Cremophor ELP buffer, probably attributed to the solubilizing agents having different effects on the nucleation and/or growth rate of the MYR crystalline phase[41]. Regarding MYR–CAF cocrystals (Fig. 5B), a higher solubility in the five surfactant solutions was also observed than that in pH 4.5 medium. Particularly, the solubility of MYR–CAF cocrystals was still increased in the lecithin buffer, suggesting that lecithin has a different solubilization capacity for different cocrystals[42]. Moreover, the remaining obtained crystalline peaks from MYR–CAF cocrystals in different solubilizing media were all consistent with those of MYR–CAF cocrystals (Fig. 6B), reflecting that this cocrystal was stable and did not dissociate to individual components even in the presence of surfactants.

To further investigate the effects of the surfactant concentration on the apparent solubility of MYR cocrystals, Tween-80 and lecithin buffer solutions were selected as the solubilizing agents owing to their different solubilization capacities (Figs. 7 and 8). The solubility of MYR–INM cocrystals was
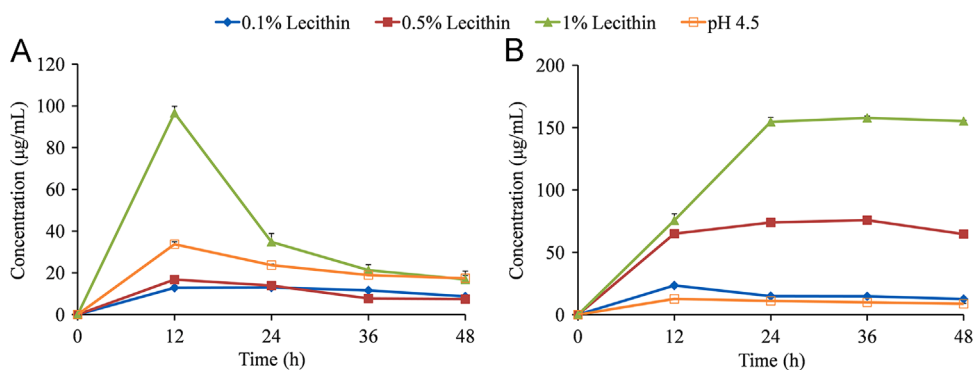
Figure 7 Apparent solubility of MYR–INM (A) and MYR–CAF (B) cocrystals in the pH 4.5 buffer containing 0.1% Lecithin (◆), 0.5% Lecithin (■), 1% Lecithin (▲), or blank pH 4.5 buffer (□) ($n = 3$).
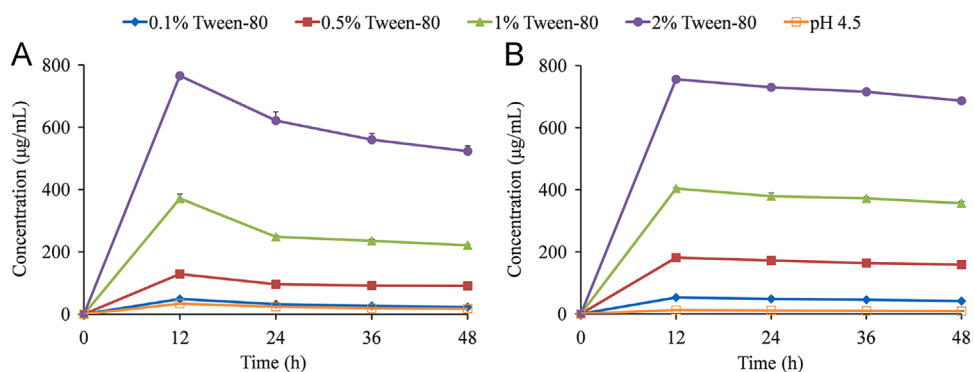
Figure 8 Apparent solubility of MYR–INM (A) and MYR–CAF (B) cocrystals in the pH 4.5 buffer containing 0.1% Tween-80 (◆), 0.5% Tween-80 (■), 1% Tween-80 (▲), 2% Tween-80 (●), or blank pH 4.5 buffer (□) ($n = 3$).

significantly improved in 1% lecithin buffer solution, and the maximum solubility was approximately three times higher than that in the pH 4.5 buffer at 12 h (Fig. 7A). However, the solubility of MYR–INM cocrystals in buffer solutions containing 0.1% and 0.5% lecithin were lower than that in pH 4.5 media, probably owing to the same reason presented in Fig. 5A. Obviously, MYR–INM cocrystals had a "spring" effect in 1% lecithin buffer solution: the supersaturation state of the cocrystal could not be maintained, leading to the cocrystal solubility decreasing over time and indicating that MYR–INM cocrystals were thermodynamically unstable in 1% lecithin buffer solution, presumably due to the surfactant concentration being below its critical stabilization concentration (CSC) value[43]. By contrast, the maximum solubility of MYR–CAF cocrystals in 1%, 0.5%, and 0.1% lecithin buffer were 5.9-fold, 5.1-fold, and 1.8-fold higher than those in pH 4.5 buffer, respectively (Fig. 7B). Thus, lecithin can enhance the solubility of MYR–INM and MYR–CAF cocrystals to different extents because the CSC values of solubilizing agents also depend on the equilibrium constant for the solubilization of CCF (K_s)[42].

Regarding Tween-80 media, the solubility of MYR–INM and MYR–CAF cocrystals increased with the increasing Tween-80 concentration, and the maximum solubility was reached at 12 h (Fig. 8). Obviously, a high concentration of Tween-80 can significantly improve the solubility of MYR–INM and MYR–CAF cocrystals, and maintain a high solubility level, probably because the viscosity of Tween-80 media was increased as the surfactant concentration increases and the nucleation rate of MYR during dissolution was suppressed.

3.1.4. Effects of ion concentration on the apparent solubility

To gain insight into the relationship between the solubility behavior and ion concentration, the apparent solubility profiles of MYR–INM and MYR–CAF cocrystals at 219.5, 400, and 600 mmol/L in pH 4.5 buffer were drawn as shown in Fig. 9. The maximum solubility values of MYR–INM cocrystals in 219.5, 400, and 600 mmol/L pH 4.5 buffers were 33.72, 37.13, and 49.50 µg/mL, respectively, and those of MYR–CAF cocrystal were 12.72, 18.84, 23.48 µg/mL, respectively. Obviously, the cocrystal solubility was dependent on the ion concentration. A similar trend was reported in the indomethacin–saccharin cocrystal, in which the solubilities were 0.72 and 1.3 mg/mL in 60 and 200 mmol/L pH 7.4 phosphate buffers, respectively[44]. Consequently, the ion concentration should be considered in the investigation of the cocrystal solubility.

3.2. Thermodynamic solubility

The thermodynamic solubility of MYR–INM cocrystal was obtained by determining the API and CCF concentrations in equilibrium with solution at the transition point[35].

The MYR–INM cocrystal is a 1:3 (API/CCF) cocrystal AB$_3$, where the API is A and the CCF is B. If a binary cocrystal of 1:3 stoichiometry dissolves in pure solvent and transforms into its individual components without further complexation, cocrystal dissociation in solution can be described by the solubility product (K_{sp})[45], and the equilibrium reactions are given according to Eq. (1):

$$AB_{3\,(solid)} \leftrightarrow A_{(solution)} + 3B_{(solution)} \tag{1}$$
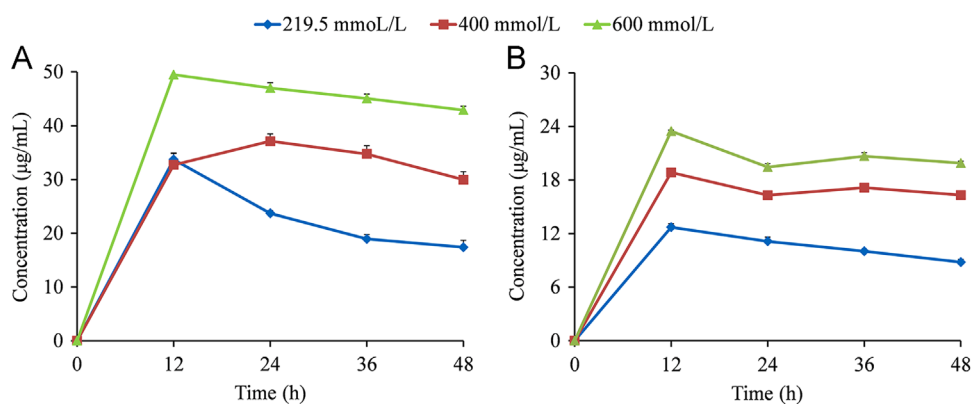
Figure 9 Apparent solubility of MYR–INM (A) and MYR–CAF (B) cocrystals in 219.5 mmol/L ($\blacklozenge$), 400 mmol/L ($\blacksquare$), 600 mmol/L ($\blacktriangle$) ($n = 3$).
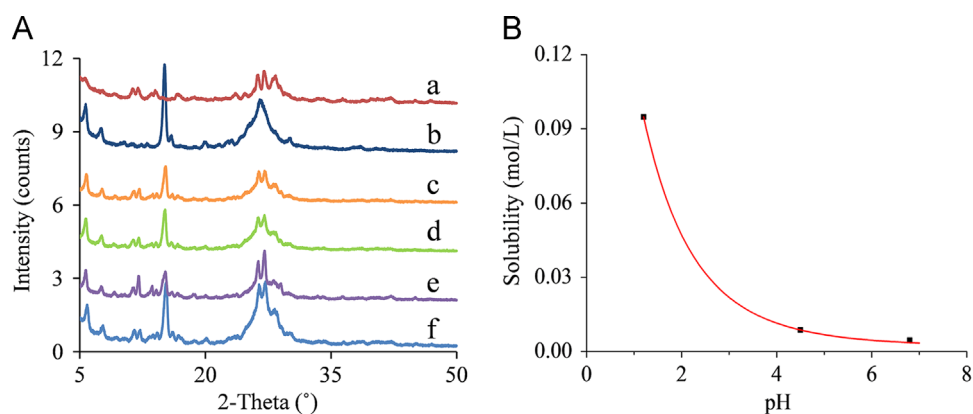
Figure 10 PXRD patterns of the residual solid after equilibrium solubility studies (A) of MYR (a) and MYR–INM (b) performed in buffer solution (37 °C) with pH 6.8 (c), pH 4.5 (d), pH 1.2 (e), and water (f). Thermodynamic solubility–pH dependence of 1:3 MYR–INM cocrystal (B). Black squares represent the measured cocrystal solubilities at transition points. Red curve was generated using models that describe cocrystal solubility–pH dependence according to Eq. (3) and the parameter values were presented in Table 1.

If the activity of the solid is equal to 1 or is constant, the cocrystal solubility can be described by a solubility product:

$$K_{sp} = [A]_{tr} \times [B]_{tr}^3 \tag{2}$$

where $[A]_{tr}$ and $[B]_{tr}$ are the molar concentrations of cocrystal components at the equilibrium. Based on the above equations, the cocrystal solubility dependence on $[H^+]$ can be expressed by

$$S_{cc} = 4\sqrt{K_{sp}/9\left(1 + K_{a1}/\left[H^+\right]\right)^3 \times \left(1 + \left[H^+\right]/K_{a2}\right)} \tag{3}$$

where K_{a1} and K_{a2} are the acid ionization constants of INM and MYR, $[H^+]$ is the hydrogen ion concentration of solution, and S_{cc} is the equilibrium solubility of MYR–INM cocrystal.

The PXRD characteristic peaks of MYR and MYR–INM cocrystals all appeared in the residual solid obtained from the thermodynamic solubility experiment in water and pH 1.2, 4.5, 6.8 buffers (Fig. 10A), indicating that the cocrystal and MYR coexisted in equilibrium with the solution at the eutectic point. The concentration of MYR and INM obtained from the supernatant represented the concentration of MYR–INM cocrystals at transition points according to the ternary phase diagram theory[46].

The transition concentrations of MYR and INM were measured at different pH buffers, while the corresponding solubility values of MYR–INM cocrystals were calculated by Eq. (3) and are presented in Table 1. The K_{sp} order in the investigated dissolution media was pH 1.2 > pH 6.8 > pH 4.5 > water, which is inversely related to the

MYR–INM cocrystal stability water > pH 4.5 > pH 6.8 > pH 1.2 (Fig. 3C). This result was in accordance with the that in the literature[12] such that the high K_{sp} values equate the high cocrystal solubility but the stability of cocrystals was opposite. The predicted solubility–pH profile of MYR–INM (1:3) cocrystals at 37 °C is shown in Fig. 10B. The theoretical solubility–pH behavior of the MYR–INM (1:3) cocrystal was in excellent agreement with the experimentally determined values. The results further illustrated that the equation we derived was sufficient to predict the equilibrium solubility of 1:3 cocrystals. Additionally, the equilibrium solubility of MYR–INM cocrystal decreases with the increasing pH values in dissolution media, likely because MYR, a weak acid ($pK_a = 6.30 \pm 0.40$), is unstable in an alkaline environment induced by the ionization of INM ($pK_a = 10.61$). Consequently, the predicted solubility curve provides the useful insight to design the cocrystal composed of acidic API and basic CCF, and the derived equation would provide guidance for the prediction of equilibrium solubility for this type of cocrystal.

3.3. Intrinsic dissolution rate (IDR)

The intrinsic dissolution rate can be used to quantitatively evaluate the dissolution behavior of compounds with a constant surface area, which is more related to *in vivo* compound dissolution dynamics than solubility[47]. Therefore, the IDR of MYR cocrystals within the first 60 min of the dissolution experiment was carried

Table 1 Transition concentration of MYR and INM, the solubility product constant (K_{sp}), and the calculated equilibrium solubility of MYR−INM cocrystal at water, pH 1.2, pH 4.5, and pH 6.8 buffer solutions.

pH	$[INM]_{tr}$ (mol/L)	$[MYR]_{tr}$ (mol/L)	K_{sp} (mol/L)	S_{cc} (mol/L)
1.2	0.040 ± 0.002	$(4.30 \pm 0.265) \times 10^{-5}$	$(2.70 \pm 0.649) \times 10^{-9}$	0.095 ± 0.005
4.5	0.019 ± 0.000	$(5.43 \pm 0.073) \times 10^{-5}$	$(3.74 \pm 0.426) \times 10^{-10}$	0.0087 ± 0.005
6.8	0.039 ± 0.001	$(3.98 \pm 0.206) \times 10^{-5}$	$(2.43 \pm 0.388) \times 10^{-9}$	0.0046 ± 0.000
Water	0.019 ± 0.000	$(3.48 \pm 0.121) \times 10^{-5}$	$(2.56 \pm 0.069) \times 10^{-10}$	0.0025 ± 0.000

Data are presented as mean $\pm$ SD ($n = 3$).

Table 2 Intrinsic dissolution rates ($\mu g/cm^2/min$) of pure MYR and its four cocrystals in 0.5% Tween-80, pure water, pH 1.2 HCl aqueous solution, pH 4.5 acetate buffer, and pH 6.8 phosphate buffer at 37 °C.

Solution/buffer	MYR	MYR−PRO	MYR−NIC	MYR−INM	MYR−CAF
0.5% Tween-80	36.37 ± 0.23	27.21 ± 0.69	27.21 ± 0.69	30.51 ± 0.00	178.67 ± 37.43
Water	9.89 ± 0.00	11.38 ± 0.93	27.66 ± 1.08	22.15 ± 9.73	14.12 ± 1.40
pH 1.2	4.46 ± 0.98	8.92 ± 1.38	5.81 ± 1.48	5.50 ± 0.69	13.56 ± 8.77
pH 4.5	2.32 ± 0.00	13.44 ± 2.86	13.42 ± 0.49	17.41 ± 0.30	16.93 ± 2.07
pH 6.8	2.65 ± 0.24	4.46 ± 0.00	6.20 ± 1.08	5.22 ± 0.24	9.68 ± 0.49

Data are presented as mean $\pm$ SD ($n = 3$).
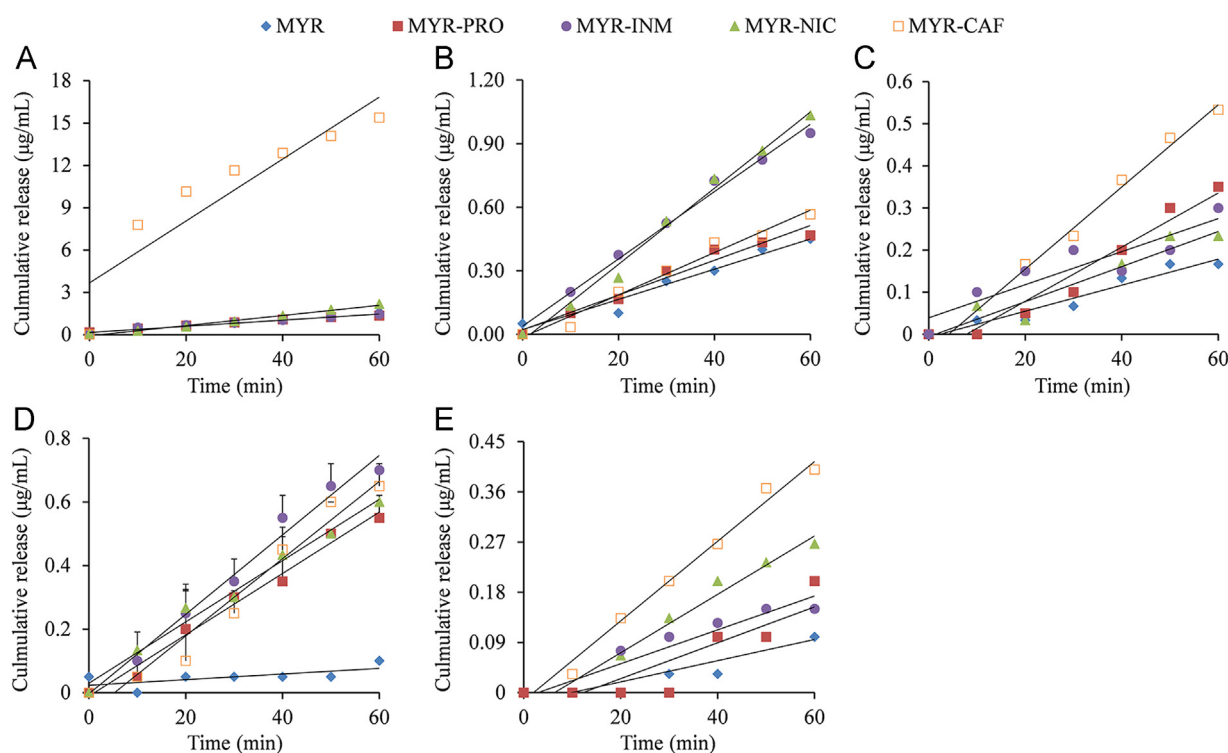
Figure 11 IDR profiles (first 60 min shown) at of MYR (♦), MYR−PRO cocrystal (■), MYR−INM cocrystal (●), MYR−NIC cocrystal (▲), and MYR−CAF cocrystal (□) performed in 0.5% Tween-80 (A), water (B), and buffer solution of pH 1.2 (C), pH 4.5 (D), pH 6.8 (E) at 37 °C ($n = 3$).

out in water and pH 1.2, 4.5, and 6.8 buffers as shown in Table 2 (the IDR curve is shown in Fig. 11). Obviously, the IDRs of MYR cocrystals in water and buffer solutions were faster than those of MYR in the same medium. In pH 4.5 buffer, the IDR of MYR cocrystals was significantly improved and increased by 5–7-fold relative to the IDR of MYR. Nevertheless, in the dissolution

medium containing Tween 80, the IDRs of MYR−INM and MYR−PRO cocrystals were slower than that of raw MYR. Similarly, this phenomenon was also observed in CBZ–NIC cocrystal[41] and is probably attributed to the interfacial barrier formed by Tween 80 because its large molecular size and shape can inhibit MYR molecules from entering the bulk solution, which will accelerate

Table 3 Crystal structure details and the refinement parameters of MYR, MYR–CAF · MeOH and MYR–INM · 2MeOH cocrystals.

Crystal structure details	MYR · H$_2$O	MYR–CAF · MeOH	MYR–INM · 2MeOH
CCDC number	1409763	1493056	1409762
Empirical formula	C$_{15}$H$_{14}$O$_{10}$	C$_{40}$H$_{40}$N$_4$O$_{21}$	C$_{37}$H$_{44}$N$_6$O$_{15}$
Formula weight	354.25	912.72	812.70
Crystal system	Monoclinic	Triclinic	Triclinic
Space group	$P2_1/c$	P-1	P-1
T/K	140(2)	293(2)	293(2)
a/Å	6.760(2)	11.0802(18)	8.0124(19)
b/Å	14.758(4)	12.2517	13.880(3)
c/Å	13.179(4)	15.674(3)	17.168(4)
α/°	90	110.273(4)	68.659(5)
β/°	96.819(5)	99.189(4)	83.225
γ/°	90	103.523(4)	77.397
V/Å^3	1305.5(7)	1871.8(5)	1734.0(7)
Z	4	2	2
D_{Cal} (mg/m^3)	1.711	1.563	1.434
μ(MoKα) (mm^{-1})	0.145	0.128	0.111
θ range	2.080 − 31.673	1.844 − 24.998	1.604 − 25.497
Reflns collected	13501	10407	9900
Independent reflns	4375	6573	6419
R_{int}	0.0974	0.0589	0.0326
GOF	0.925	1.046	1.100
R_1, $I > 2\sigma$ (I)	0.0619	0.0876	0.0775
wR_2, $I > 2\sigma$ (I)	0.1402	0.1780	0.1870
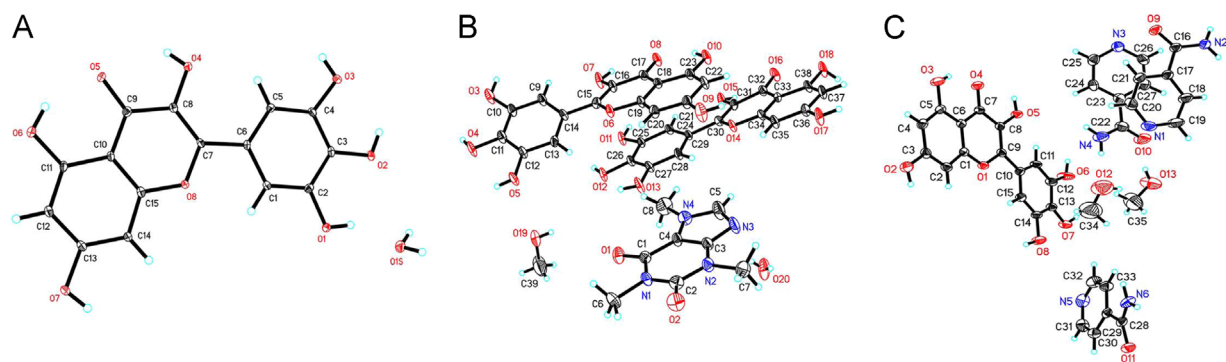
Figure 12 The atoms number of the asymmetric unit for MYR · H$_2$O (A), MYR–CAF · MeOH (B) and MYR–INM · 2MeOH cocrystals (C).

nucleation and/or the growth of the MYR molecule on the solid surface. In summary, the formation of cocrystals can accelerate the intrinsic dissolution rate of poorly soluble MYR, which presumably would result in better absorption in the *in vivo* environment, especially in pH 4.5 buffer.

3.4. Single-crystal X-ray diffraction

The crystal structures of MYR · H$_2$O, MYR–CAF · MeOH and MYR–INM · 2MeOH cocrystals were determined by single-crystal X-ray diffraction, and the crystallographic data and details of refinement are summarized in Table 3. In addition, the atoms number of the asymmetric unit for MYR · H$_2$O, MYR–CAF · MeOH and MYR–INM · 2MeOH cocrystals are shown in Fig. 12 and the hydrogen bond parameters are provided in Supporting Information.

MYR · H$_2$O crystallizes in the $P2_1$/c space group and contains the asymmetric unit with one MYR molecule and one water molecule (Fig. 13). The adjacent MYR molecules are linked by water molecules through O$_7$· · ·H$_{1S}$−O$_{1S}$ (2.16 Å) and O$_1$−H$_{1A}$· · ·O$_{1S}$ (1.89 Å) to form an MYR chain. The two parallel MYR chains are arranged as a 1D chain structure *via* O$_7$−H$_7$· · ·O$_1$ (1.94 Å) to form an MYR monolayer. Meanwhile, the O$_6$−H$_6$···O$_5$ (1.89 Å) intramolecular hydrogen bonds is formed among MYR molecules. Noticeably, the MYR monolayer is further fabricated into two-dimensional H-bonding network using O$_3$−H$_3$· · ·O$_5$ (1.84 Å) and O$_4$−H$_4$· · ·O$_3$ (2.18 Å), which are additionally extended into a three-dimensional architecture throughout the crystal structure *via* weak interactions (Supporting Information Table S1).

MYR-CAF · MeOH crystallizes in the triclinic, P-1 space group, with the asymmetric unit containing two MYR molecules, one CAF molecule, one water molecule, and one methanol molecule (Fig. 14). An important feature of this system includes two structural hierarchies (1D chains): MYR molecules are linked together through two intermolecular hydrogen bonds, O$_5$−H$_5$O$_{10}$ (1.96 Å) and O$_{18}$· · ·H$_{13}$−O$_{13}$ (2.03 Å), to form an MYR
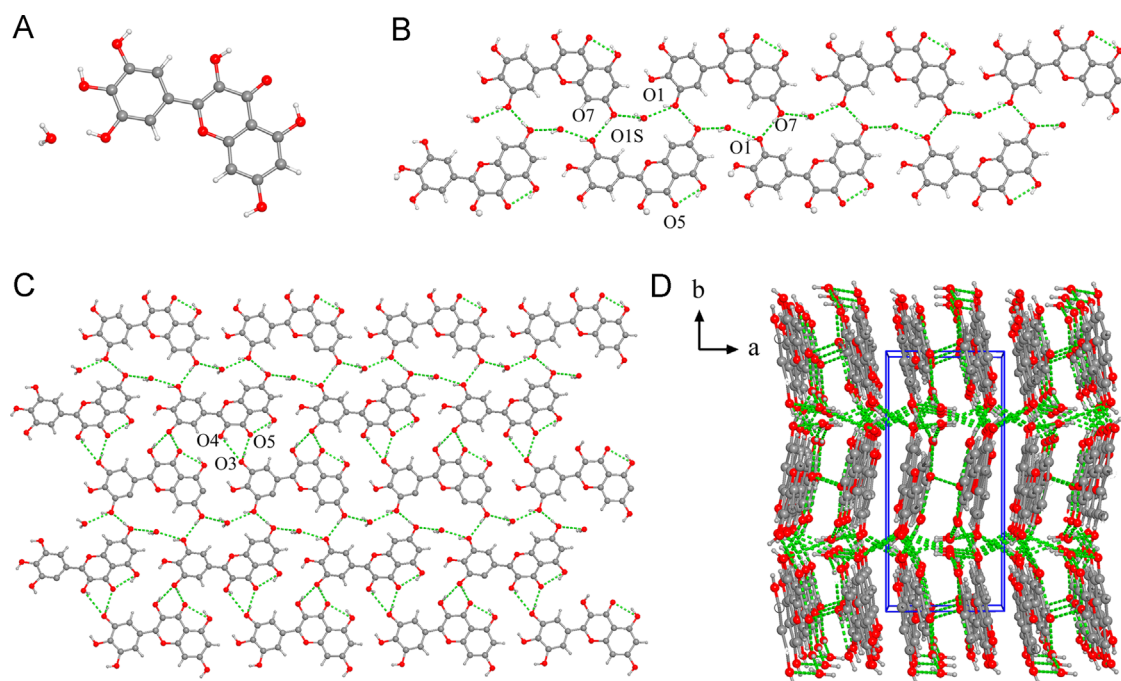
Figure 13 Unit cell (a), 1D chain (b), 2D sheet (c), 3D structure (d) for MYR $\cdot$ H_2O.
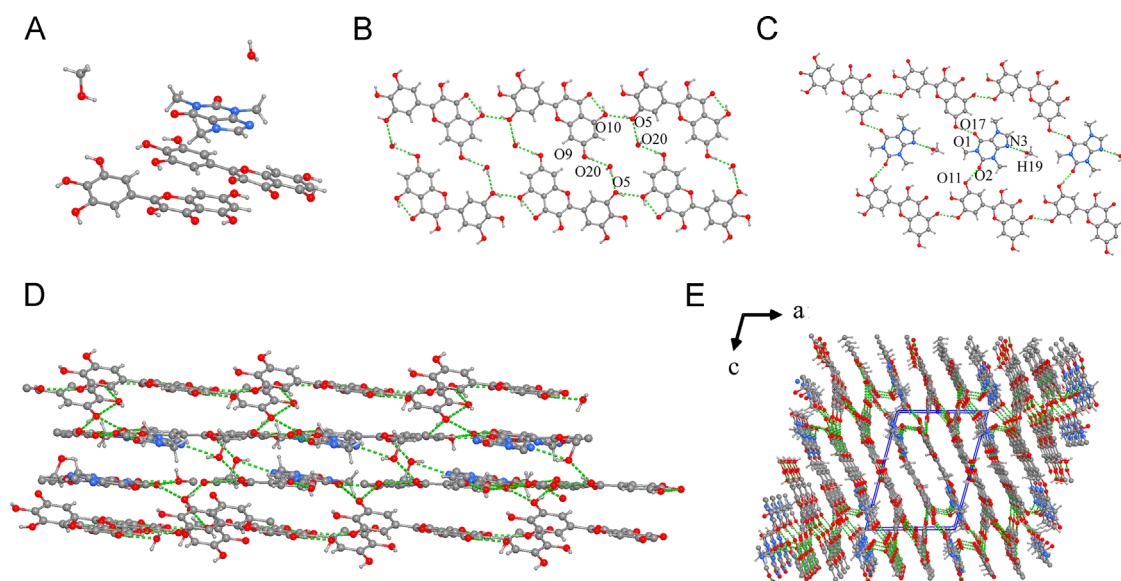
Figure 14 Unit cell (a), 1D chain (b) and (c), 2D sheet (d), 3D structure (e) with double layers for MYR-CAF $\cdot$ MeOH cocrystal.

monolayer and the MYR and CAF molecules form the other layer; meanwhile, CAF molecules play a bridging role connecting the adjacent two MYR molecules, forming intermolecular hydrogen bonds: $O_1 \cdots H_{17}-O_{17}$ (1.86 Å) with one MYR molecule and $O_2 \cdots H_{11}-O_{11}$ (1.93 Å) with the other MYR molecule. Furthermore, methanol molecules are introduced to interact with CAF and MYR molecules through $N_3 \cdots H_{19}-O_{19}$ (2.08 Å), $O_{15}-H_{15} \cdots O_{19}$ (1.85 Å), and $O_{16} \cdots H_{19}-O_{19}$ bonds (1.85 Å). In addition, MYR and water molecules are connected to each other *via* an $O_{20}-H_{20B} \cdots O_9$ bond (2.59 Å). Notably, all of the MYR molecules also form $O_{16} \cdots H_{18}-O_{18}$ intramolecular hydrogen bonds. The two adjacent 1D chains are further connected *via* interlayer

hydrogen bonds ($O_4-H_4 \cdots O_{11}$, (2.18 Å); $O_3-H_3 \cdots O_{16}$, (1.98 Å); $O_3 \cdots H_{12}-O_{12}$, (2.06 Å)) to generate a two-dimensional (2D) bilayer. The two MYR-CAF monolayers are continuously linked, and then, their flanks are connected to MYR monolayers to form a three-dimensional (3D) structure (Supporting Information Table S2).

MYR-INM $\cdot$ 2MeOH crystallizes in the triclinic, *P*-1 space group, with the asymmetric unit containing one MYR molecule, two methanol molecules, and three INM molecules (Fig. 15) that are connected through $O_2-H_2 \cdots N_3$ (1.91 Å), $O_8-H_8 \cdots O_{11}$ (1.88 Å), and $N_6-H_{6B} \cdots O_8$ (2.45 Å) intermolecular hydrogen bonds; meanwhile, MYR forms the intermolecular hydrogen
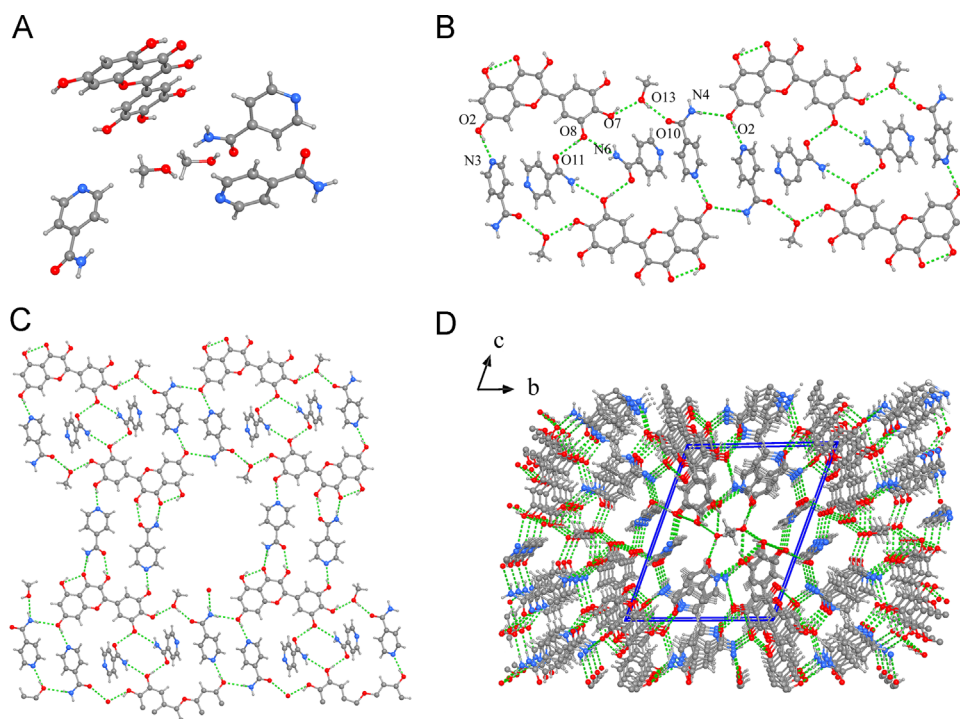
Figure 15 Unit cell (a), 1D chain (b), 2D sheet (c), 3D structure (d) for MYR-INM·2MeOH cocrystal.

bonds *via* $O_4\cdots H_3-O_3$ (1.90 Å). In addition, one methanol molecule serves as a bridge to connect MYR and INM dimers together by $O_7-H_7\cdots O_{13}$ (1.93 Å) and $O_{13}-H_{13}\cdots O_{10}$ (1.91 Å); the other methanol molecule is linked with MYR molecule through $O_6\cdots O_{12}-H_{12}$. The two-unit cells form a repeated sheet, and the two adjacent sheets are connected by $N_4-H_4\cdots O_2$ (2.26 Å) interchain hydrogen bonds to form a one-dimensional (1D) chain. The 1D chains are further linked by INM molecules ($O_6-H_6\cdots N_1$, (1.86 Å); $O_4\cdots N_2-H_{2A}$, (2.31 Å); $O_5-H_5\cdots O_9$, (2.06 Å)) and methanol molecules ($O_6\cdots O_{12}-H_{12}\cdots N_4$, (2.04 Å)) through inter-layer hydrogen to form a 2D bilayer, which is additionally extended into a three-dimensional architecture *via* relatively weak interactions (Supporting Information Table S3).

Based on the above mentioned, MYR cocrystals can alter the arrangements of MYR molecules in the raw form and break the packing density of adjacent layers, leading to the increased intermolecular distance, so that the solvent molecule is liable to penetrate the MYR molecule structure. In detail, the MYR molecules in the MYR crystal interact with each other through $O_1\cdots H_7-O_7$, and the corresponding $O\cdots H$ distance is 1.94 Å, while the spatial distance for MYR molecules in the MYR–CAF·MeOH cocrystal is increased by intermolecular hydrogen bonding ($O_1\cdots H_{17}-O_{17}$, (1.86 Å); $O_2\cdots H_{11}-O_{11}$, (1.93 Å)); regarding the MYR–INM·2MeOH cocrystal, the spatial distance for the MYR molecules is increased by intermolecular hydrogen bonding ($O_2-H_2\cdots N_3$, (1.91 Å); $O_7-H_7\cdots O_{13}$, (1.93 Å); $O_{13}-H_{13}\cdots O_{10}$, (1.91 Å)). Additionally, the methanol or water molecule is introduced to facilitate the inclusion of solvent molecules in the crystal lattice[48], thereby increasing the cocrystal solubility. Significantly, the CCFs play a crucial role in the arrangement of the cocrystal spatial structure, and crystal structure analysis can visually elucidate the physicochemical properties of cocrystals, which would be beneficial for the reasonable design of

pharmaceutical cocrystals and promote their further application in the drug delivery field.

4. Conclusions

In buffer solution, the kinetic solubility of MYR cocrystals, based on the phase transformation and equilibrium reactions for cocrystal dissociation, which are regulated by the concentration of hydrogen ions or hydroxyl ions in solution, can be modulated by pH and CCF ionization; in pure water, the kinetic solubility of MYR cocrystals dominantly depends on the solubility of CCFs. Moreover, the solubility of MYR cocrystals can be increased in a concentration dependent fashion according to the surfactant or ion concentration. The thermodynamic solubility of MYR–INM (1:3) cocrystals decreased with the increasing pH value of the dissolution media. The IDR of MYR cocrystals was faster than that of pure MYR in the same dissolution and increased 5–7 times in pH 4.5 buffer. The alternate arrangements of MYR and INM/CAF molecules and the increased intermolecular distance are possible explanations for the enhanced MYR cocrystal solubility. The present study provides an in-depth understanding of cocrystal solubility, which will promote the development of formulations for pharmaceutical cocrystals.

Appendix A. Supporting information

Supplementary data associated with this article can be found in the online version at https://doi.org/10.1016/j.apsb.2018.09.008.

References

1. Qiao N, Li MZ, Schlindwein W, Malek N, Davies A, Trappitt G. Pharmaceutical cocrystals: an overview. *Int J Pharm* 2011;**419**:1–11.
2. Skorupska E, Kazmierski S, Potrzebowski MJ. Solid state NMR characterization of ibuprofen:nicotinamide cocrystals and new idea for controlling of release of the drugs embedded into mesoporous silica particles. *Mol Pharm* 2017;**14**:1800–10.
3. Li S, Yu T, Tian Y, McCoy CP, Jones DS, Andrews GP. Mechanochemical synthesis of pharmaceutical cocrystal suspensions via hot melt extrusion: feasibility studies and physicochemical characterization. *Mol Pharm* 2016;**13**:3054–68.
4. Korotkova EI, Kratochvíl B. Pharmaceutical cocrystals. *Proc Chem* 2014;**10**:473–6.
5. Shekhawat PB, Pokharkar VB. Understanding peroral absorption: regulatory aspects and contemporary approaches to tackling solubility and permeability hurdles. *Acta Pharm Sin B* 2017;**7**:260–80.
6. Smith AJ, Kavuru P, Wojtas L, Zaworotko MJ, Shytle RD. Cocrystals of quercetin with improved solubility and oral bioavailability. *Mol Pharm* 2011;**8**:1867–76.
7. Sravani E, Mannava MKC, Kaur D, Annapurna BR, Khan RA, Suresh K, et al. Preclinical bioavailability–bioequivalence and toxico–kinetic profile of stable succinc acid cocrystal of temozolomide. *Curr Sci India* 2015;**108**:1097–106.
8. U.S. Department of Healthand Human Services, Food and Drug Administration, Center for Drug Evaluation and Research (CDER). Regulatory classification of pharmaceutical co-crystals. Guidance for industry. 2013. Available from: ⟨http://www.fda.gov/downloads/Drugs/GuidanceComplianceRegulatoryInformation/Guidances/UCM516813.pdf⟩.
9. Gadade DD, Pekamwar SS. Pharmaceutical cocrystals: regulatory and strategic aspects, design and development. *Adv Pharm Bull* 2016;**6**:479–94.
10. Bavishi DD, Borkharia CH. Spring and parachute: how cocrystals enhance solubility. *Prog Cryst Growth Charact Mater* 2016;**62**:1–8.
11. Greco K, Bogner R. Solution-mediated phase transformation: significance during dissolution and implications for bioavailability. *J Pharm Sci* 2012;**101**:2996–3018.
12. Good DJ, Rodríguez-Hornedo N. Solubility advantage of pharmaceutical cocrystals. *Cryst Growth Des* 2009;**9**:2252–64.
13. Grossjohann C, Eccles KS, Maguire AR, Lawrence SE, Tajber L, Corrigan OI, et al. Characterisation, solubility and intrinsic dissolution behaviour of benzamide: dibenzyl sulfoxide cocrystal. *Int J Pharm* 2012;**422**:24–32.
14. Healy AM, McCarthy LG, Gallagher KM, Corrigan OI. Sensitivity of dissolution rate to location in the paddle dissolution apparatus. *J Pharm Pharmacol* 2002;**54**:441–4.
15. Thakuria R, Delori A, Jones W, Lipert MP, Roy L, Rodríguez-Hornedo N. Pharmaceutical cocrystals and poorly soluble drugs. *Int J Pharm* 2013;**453**:101–25.
16. Huang N, Rodríguez-Hornedo N. Engineering cocrystal thermodynamic stability and eutectic points by micellar solubilization and ionization. *CrystEngComm* 2011;**13**:5409–22.
17. Semwal DK, Semwal RB, Combrinck S, Viljoen A. Myricetin: a dietary molecule with diverse biological activities. *Nutrients* 2016;**8**:1–31.
18. Sultana B, Anwar F. Flavonols (kaempferol, quercetin, myricetin) contents of selected fruits, vegetables and medicinal plants. *Food Chem* 2008;**108**:879–84.
19. Dang Y, Lin Gb, Xie Y, Duan JZ, Ma P, Li GW, et al. Quantitative determination of myricetin in rat plasma by ultra performance liquid chromatography tandem mass spectrometry and its absolute bioavailability. *Drug Res* 2014;**64**:516–22.
20. Yao YS, Lin GB, Xie Y, Ma P, Li GW, Meng QC, et al. Preformulation studies of myricetin: a natural antioxidant flavonoid. *Pharmazie* 2014;**69**:19–26.
21. Shan N, Zaworotko MJ. The role of cocrystals in pharmaceutical science. *Drug Discov today* 2008;**13**:440–6.
22. Liu MY, Hong C, Yao YS, Shen HY, Ji G, Li GW, et al. Development of a pharmaceutical cocrystal with solution crystallization technology: preparation, characterization, and evaluation of myricetin–proline cocrystals. *Eur J Pharm Biopharm* 2016;**107**:151–9.
23. Liu MY, Hong C, Li GW, Ma P, Xie Y. The generation of myricetin–nicotinamide nanococrystals by top down and bottom up technologies. *Nanotechnology* 2016;**27**:395601.
24. Mureşan-Pop M, Chiriac LB, Martin F, Simon S. Novel nutraceutical myricetin composite of enhanced dissolution obtained by co-crystallization with acetamide. *Compos Part B-Eng* 2016;**89**:60–6.
25. Sowa M, Ślepokura K, Matczak-Jon E. A 1:1 pharmaceutical cocrystal of myricetin in combination with uncommon piracetam conformer: X-ray single crystal analysis and mechanochemical synthesis. *J Mol Struct* 2014;**1058**:114–21.
26. Zhang YN, Yin HM, Zhang Y, Zhang DJ, Su X, Kuang HX. Cocrystals of kaempferol, quercetin and myricetin with 4,4′-bipyridine: crystal structures, analyses of intermolecular interactions and antibacterial properties. *J Mol Struct* 2017;**1130**:199–207.
27. Hong C, Xie Y, Yao YS, Li GW, Yuan XR, Shen HY. A novel strategy for pharmaceutical cocrystal generation without knowledge of stoichiometric ratio: myricetin cocrystals and a ternary phase diagram. *Pharm Res* 2015;**32**:47–60.
28. Kuminek G, Cao FJ, Bahia de Oliveira da Rocha A, Gonçalves Cardoso S, Rodríguez-Hornedo N. Cocrystals to facilitate delivery of poorly soluble compounds beyond-rule-of-5. *Adv Drug Deliv Rev* 2016;**101**:143–66.
29. Babu NJ, Nangia A. Solubility advantage of amorphous drugs and pharmaceutical cocrystals. *Cryst Growth Des* 2011;**11**:2662–79.
30. Shiraki K, Takata N, Takano R, Hayashi Y, Terada K. Dissolution improvement and the mechanism of the improvement from cocrystallization of poorly water-soluble compounds. *Pharm Res* 2008;**25**:2581–92.
31. Maheshwari C, AndréV, Reddy S, Roy L, Duarte T, Rodríguez-Hornedo N. Tailoring aqueous solubility of a highly soluble compound via cocrystallization: effect of coformer ionization, pH$_{max}$ and solute–solvent interactions. *CrystEngComm* 2012;**14**:4801–11.
32. Roy L, Lipert MP, Rodríguez-Hornedo N. Co-crystal solubility and thermodynamic stability. In: Johan W, Luc Q, editors. *Pharmaceutical Salts and Co-crystals*. London: the Royal Society of Chemistry; 2012. p. 247–79.
33. Cardew PT, Davey RJ. The kinetics of solvent-mediated phase transformations. *Proc R Soc A-Math Phys* 1985;**398**:415–28.
34. Brouwers J, Brewster ME, Augustijns P. Supersaturating drug delivery systems: the answer to solubility-limited oral bioavailability?. *J Pharm Sci* 2009;**98**:2549–72.
35. Alhalaweh A, Roy L, Rodríguez-Hornedo N, Velaga SP. pH-dependent solubility of indomethacin–saccharin and carbamazepine–saccharin cocrystals in aqueous media. *Mol Pharm* 2012;**9**:2605–12.
36. Reddy LS, Bethune SJ, Kampf JW, Rodríguez-Hornedo N. Cocrystals and salts of gabapentin: ph dependent cocrystal stability and solubility. *Cryst Growth Des* 2009;**9**:378–85.
37. Ozturk SS, Palsson BO, Dressman JB. Dissolution of ionizable drugs in buffered and unbuffered solutions. *Pharm Res* 1988;**5**:272–82.

38. Putra OD, Umeda D, Nugraha YP, Furuishi T, Nagase H, Fukuzawa K, et al. Solubility improvement of epalrestat by layered structure formation *via* cocrystallization. *CrystEngComm* 2017;**19**:2614–22.

39. Söderlind E, Karlsson E, Carlsson A, Kong R, Lenz A, Lindborg S, et al. Simulating fasted human intestinal fluids: understanding the roles of lecithin and bile acids. *Mol Pharm* 2010;**7**:1498–507.

40. Huang N, Rodríguez-Hornedo N. Engineering cocrystal solubility, stability, and pH_{max} by micellar solubilization. *J Pharm Sci* 2011;**100**:5219–34.

41. Li MZ, Qiao N, Wang K. Influence of sodium lauryl sulfate and tween 80 on carbamazepine–nicotinamide cocrystal solubility and dissolution behaviour. *Pharmaceutics* 2013;**5**:508–24.

42. Huang N, Rodríguez-Hornedo N. Effect of micellar solubilization on cocrystal solubility and stability. *Cryst Growth Des* 2010;**10**:2050–3.

43. Bhardwaj S, Lipert M, Bak A. Mitigating cocrystal physical stability liabilities in preclinical formulations. *J Pharm Sci* 2017;**106**:31–8.

44. Basavoju S, Boström D, Velaga SP. Indomethacin–saccharin cocrystal: design, synthesis and preliminary pharmaceutical characterization. *Pharm Res* 2008;**25**:530–41.

45. Good DJ, Rodríguez-Hornedo N. Solubility advantage of pharmaceutical cocrystals. *Cryst Growth Des* 2009;**9**:2252–64.

46. Jayasankar A, Roy L, Rodríguez-Hornedo N. Transformation pathways of cocrystal hydrates when coformer modulates water activity. *J Pharm Sci* 2010;**99**:3977–85.

47. Shevchenko A, Bimbo LM, Miroshnyk I, Haarala J, Jelínková K, Syrjänen K, et al. A new cocrystal and salts of itraconazole: comparison of solid-state properties, stability and dissolution behavior. *Int J Pharm* 2012;**436**:403–9.

48. Zhu BQ, Zhang Q, Wang JR, Mei XF. Cocrystals of baicalein with higher solubility and enhanced bioavailability. *Cryst Growth Des* 2017;**17**:1893–901.